Supplementary material

Network model

The derivation of functional connectivity and the subsequent mathematical modelling follows from multiple works looking for an optimal resection site using intracranial EEG [1, 2, 3]. In order to derive functional networks from the ViEEG time-series, 20 second epochs of seizure data containing clear ictal waveforms were chosen by MC, SV and CP. In the event that a seizure was shorter than 20s, the whole seizure was used. In the event that the entire recording showed semi-continuous ictal runs, epochs closer to the onset of the seizure were favoured (Supplementary Table 4). We then down-sampled the data to 512 Hz and band-pass filtered between 1 and 25 Hz using a 4th order Butterworth filter. We used these epochs to compute univariate iterated amplitude adjusted Fourier transform surrogates for each epoch. We used 199 surrogates unless otherwise noted. Each epoch was then divided into 10 minimally overlapping sub-segments of 0.25 times the length of the original epoch. This resulted in 10 subsegments of the original time series and usually 1990 subsegments for the surrogates. We considered two functional connectivity methods: (1) Pearson correlation coefficient between amplitude envelopes (AEC) [4, 5] and (2) mutual information (MI) [1, 6, 7]. In order to accurately estimate the mutual information, we used the publicly available MILCA package [6]. To make the analyses computationally tractable, we reduced the number of surrogates to 19 when using mutual information to infer functional connectivity. We then used the Mann-Whitney-Wilcoxon U-test to assess whether the connections were significantly larger in the original time series (ρ_0) against the surrogate time series' (ρ_{surr}). The surrogate-corrected connectivity matrix is as follows:

$$CC_{ij} = \frac{< \rho_{0_{ij}} > - < \rho_{surr_{ij}} >}{1 - < \rho_{surr_{ij}} >} h_{ij},$$

where $h = 1$ if the null hypothesis of the statistical test was rejected, or $h = 0$ otherwise. $< >$ indicates the median values over subsegments and surrogates.

We considered each of the nodes in each in ViEEG as connected neural masses using the theta model [2, 3]. The phase of each node follows the ODE:

$$\theta_j' = (1 - cos) + \left(1 + cos\left(\theta_j\right)\right) I_j(t),$$

where the inputs are described by $I_j(t)$:

$$I_j(t) = I_0^j + \xi^j(t) + \frac{K}{N}\sum_{i \neq j} \quad CC_{ij}(1 - cos(\theta_i - \theta_i^s)) \, .$$

The index j denotes the node j, N is the total number of nodes, $I_0^j + \xi^j(t)$ is Gaussian noise, K is the global scaling parameter, a_{ij} is the $i, j - th$ entry in the functional connectivity network, and θ_i^S is the steady state of node i. Each node is initially in a 'normal state', which is a stable fixed point for the system, but can transition into the 'seizure state', a limit cycle, by passage through a saddle-node on invariant circle (SNIC) bifurcation.

As in Goodfellow *et al.* (2016), we quantified the dynamics of the system using the notion of brain network ictogenicity BNI, which is the average fraction of time that each node spends in the seizure state. This value is obtained by computing the dynamical system over a long period of time (46 timesteps), with multiple runs to mitigate the effects of noise (128 noise runs) and averaging the time spent in the seizure state over all nodes, times, and runs. For a given network, the value of BNI will depend on the global scaling parameter, K. Therefore, for the full network, we find the value of K such that $BNI = 0.5$. We then use this value of K when simulating the surgical resection, as follows. In order to simulate surgical resection, we quantify the node ictogenicity (NI) of each node. To do this, we remove each node i individually and rerun the dynamical system to calculate a new BNI value, BNI_{post}^i. The value NI is then given by:

$$NI^i = \frac{BNI_{pre} - BNI_{post}^i}{BNI_{pre}} \, ,$$

where $BNI_{pre} = 0.5$. If BNI_{post}^i is small (aka NI^i is large), then the node is considered ictogenic, or a candidate for resection, because removing it as the effect of reducing the fraction of time the dynamical system spends in the seizure state. Again, we run each of these 'virtual resections' 128 times for 46 timesteps. This generates a distribution of NI^i values for each node removed. We then used a Mann-Whitney-Wilcoxon U-test and Bonferroni-Holms multiple comparisons correction to assess whether NI^i is greater than the NI over all removed nodes. The nodes i that have significantly large and positive NI^i become the VIZ.

Features of ictal ViEEG signals

We visually inspected each ViEEG seizure and ensured all ViEEG seizures analysed by dynamical network models have 1) visible transition from background activity to ictal waveforms that is aligned in time with seizure onset annotated by C.P. using MEG sensor signals and 2) distinctive morphological features and spatial distribution of ictal waveforms that are similar to seizures recorded by iEEG, if iEEG is done. Example ictal ViEEG signals from each seizure are presented in Supplementary Figs. 4-15. Ictal ViEEG signals were plotted in a 10-second window using seizure onset as time zero and 2 seconds before seizure onset and 8 seconds after seizure onset. As shown in Fig. 2 (main paper), ictal ViEEG signals present distinctive ictal rhythms akin to an ictal event independently recorded by iEEG. This finding supports the previous studies that MEG can 'see' activities from deep structures [8, 9, 10, 11] and seizures can be reconstructed from those sources with similar features to an iEEG seizure.

Considerations for ViEEG locations

iEEG locations play a critical role in clinically characterising the EZ. Therefore, whether ViEEG locations affect our proposed model to characterise the EZ non-invasively is an important question to ask. As discussed in the main paper, ViEEG locations are defined to extensively cover the early-, mid-, and late-phase MSL solutions as well as the entirety of the resection margin. It is important to note that the choice of location, shape and orientation of ViEEG does not take into account any other information (such as shape of resection or pathology) – they are defined in a non-regularised fashion to sufficiently sample the targeted brain areas along the cortical surface (like subdural grid electrodes) and linearly (like stereotactic depth electrodes) along deep cortical structures, such as hippocampal structures. As well, ViEEG and network models do not require the resection margin and MSL solutions to be in any specific locations within the ViEEG, such as the centre of the ViEEG. When defining the ViEEG, we always ensure there is sufficient brain tissue between the ViEEG boundary and the boundary of resection and MSL solutions. In Patient 5 (Supplementary Fig. 1A), we demonstrate the same AEC-VIZ 'hotspot' location is found by two different ViEEGs modelled independently. ViEEG1 and ViEEG2 grid and depth electrode set-ups differ but the resulting left baso-mesial temporal VIZ localisations are similar. Providing the area of interest is covered for the VIZ analysis, these results suggest our proposed model is less likely to be affected by how the ViEEG is initially defined. A second example is given by Patient 11 (Supplementary Fig. 1B), where a 4-by-4 grid like ViEEG is defined at the contralateral temporal area (less clinically concerning) together with a 10-by-10 grid covering the resection margin and MSL locations. The additional 16 nodes from the 4-by-4 grid covering a contralateral brain area does not affect the model in identifying the VIZ hotspot location that is concordant with the iEEG SOZ.

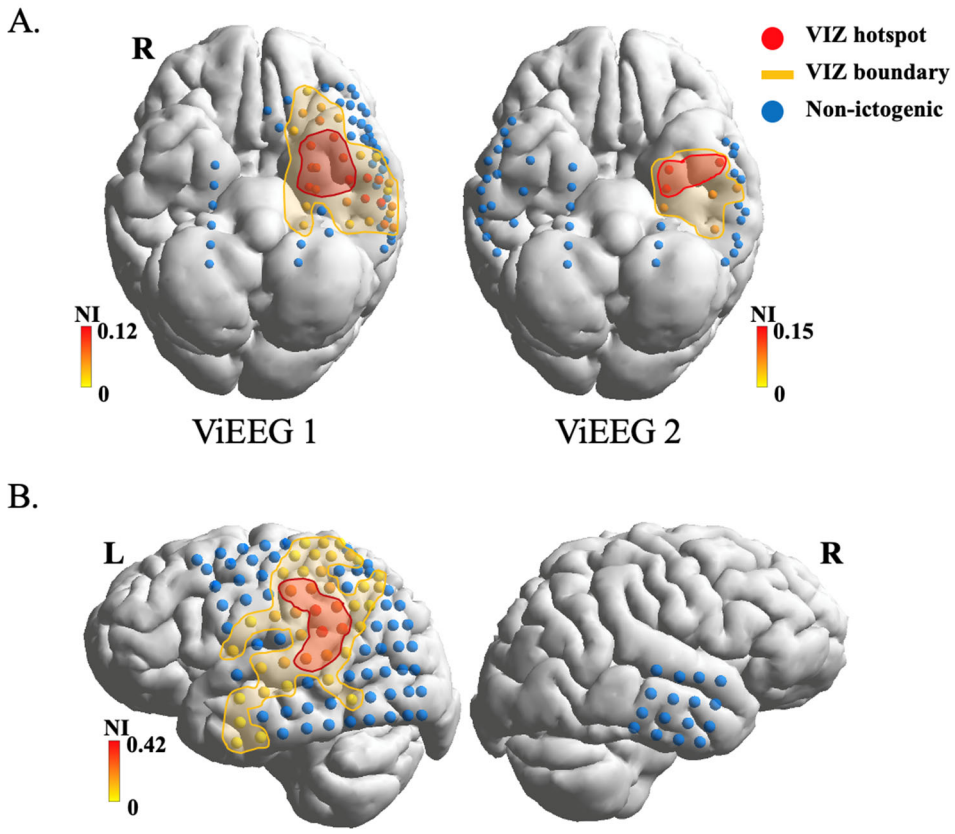

Supplementary Figure 1. Variation in the initial ViEEG set-up appears to have minimal effect on the VIZ result, providing the area of interest is covered. The VIZ for Patient 5 (Supplementary Fig. 1A) remains left temporal baso-mesial despite differences in the initial ViEEG configuration. The VIZ for Patient 11 (Supplementary Fig. 1B) is unaffected by the introduction of a contralateral (right) 16-electrode ViEEG grid. VIZ boundary and hotspot results have been derived from the AEC-VIZ method.

ViEEG signal reconstruction

We defined ViEEG electrodes to cover brain areas that have been source localised using MEG (early, mid and late) from the previous publication [10] and ensured to contain the entire resection bed with sufficient margin between the boundaries of resection and ViEEG electrodes. In other words, ViEEG was only guided by MEG source localisation and resection margins (and not the iEEG array or other clinical information). Next, we attempted to reconstruct ictal source signals of each ViEEG electrode akin to what is recorded invasively with iEEG. Bad MEG channels were identified and omitted from raw MEG recordings during and after data acquisition. A temporal extension to signal source separation (tSSS) was then applied to MEG sensor signals using *Maxfilter v2.2.10-15* (Elekta Oy) for interference suppression. After tSSS, a notch filter was applied to remove line noise at 50 Hz and its harmonics up to 300 Hz and an IIR filter to bandpass filter signals between 0.1 and 200 Hz.

Pre-processed MEG signals were then segmented into epochs of 10 minutes before seizure onset and the whole seizure event from seizure onset to seizure termination. Onset and offset of each seizure were annotated by C.P. and also reported in the previous publication [10]. Long epochs and broad frequency bands were used for source reconstruction to more reliably estimate noise covariance matrices and alleviate the suppression of correlated sources by beamformer techniques [12, 13]. Empirically, we also found shorter epochs often resulted in less distinctive morphologies and more smeared spatial distributions of ictal source signals.

A scalar beamformer technique was employed to reconstruct ictal ViEEG signals [14]. The orientation of each dipolar source was computed to maximise source power [15, 16]. Beamformer techniques have been used to successfully reconstruct source signals for various applications at high spatial resolution, particularly in the context of MEG virtual electrodes [16, 17]. More specifically, given a ViEEG electrode, we constructed a set of beamformer weights that spatially filter source activity at this location without contribution from other sources. We used an implementation of linearly constrained minimum variance (LCMV) beamformer with orientations optimised by maximal source power from MNE-Python Version 0.19.0 [18]. To construct a beamformer at each ViEEG electrode, the data covariance matrix was estimated using the whole seizure event (from seizure onset to seizure termination), while the noise covariance matrix was estimated using a pre-seizure segment (i.e., -600 second to -10 second

if seizure onset is defined as 0 second). The pre-seizure segment had been visually inspected to ensure no ictal activity is included. We used realistic boundary element method (BEM) models generated from individualised MRI scans to compute forward solutions. Triangulated mesh surfaces of inner-skull and pial surface were generated using the patient-specific MRI scan, Freesurfer [19] and CURRY 8® (Compumedics Neuroscan®, Hamburg) software. After source signal reconstruction, we visually inspected ictal ViEEG signals and identified 25/36 seizures from 12 patients that presented a distinctive morphology and spatial distribution from background activity. These 25 seizures were then analysed by dynamical network models.

Volume conduction and functional networks

Volume conduction introduces source signal leakage that affects source signal reconstruction and structures of time-evolving EEG and MEG source networks. We explored extensively in parameter space to optimise the spatial resolution and signal strength of ictal ViEEG signals. However, these efforts are not guaranteed to completely remove spurious interactions from MEG source networks. Palva *et al*. (2018) using simulations and realistic head models demonstrated that the currently available methods cannot completely remove spurious connections. In other words, when there is a true connection, spurious connections always accompany. Another study from Hincapie *et al.* (2017) suggests different source reconstruction techniques, size and locations of correlated sources also change the extent to which field leakage impacts source signals. However, a limitation of both studies is that only two genuinely correlated sources were taken into account in their simulations [4, 20]. Moreover, the connectivity methods used to reduce instantaneous phase synchrony may have been too conservative to preserve important network structures, particularly if more than two sources genuinely correlate. For iEEG studies and our proposed ViEEG approach, the assumption of only two correlated sources in the network is less likely to be valid when a seizure occurs.

Because we aimed to explore clinical biomarkers that pre-surgically characterise the EZ in a non-invasive fashion, the connectivity methods we employed did not remove instantaneous spurious connections in an effort to better preserve key functional network structures [21]. Note also that we did not attempt to interpret our findings in the context of neural mechanisms related to seizure generation. Biomarkers and limitations are discussed with the support of statistical analysis (main paper and below).

Different thresholds to define the VIZ hotspot

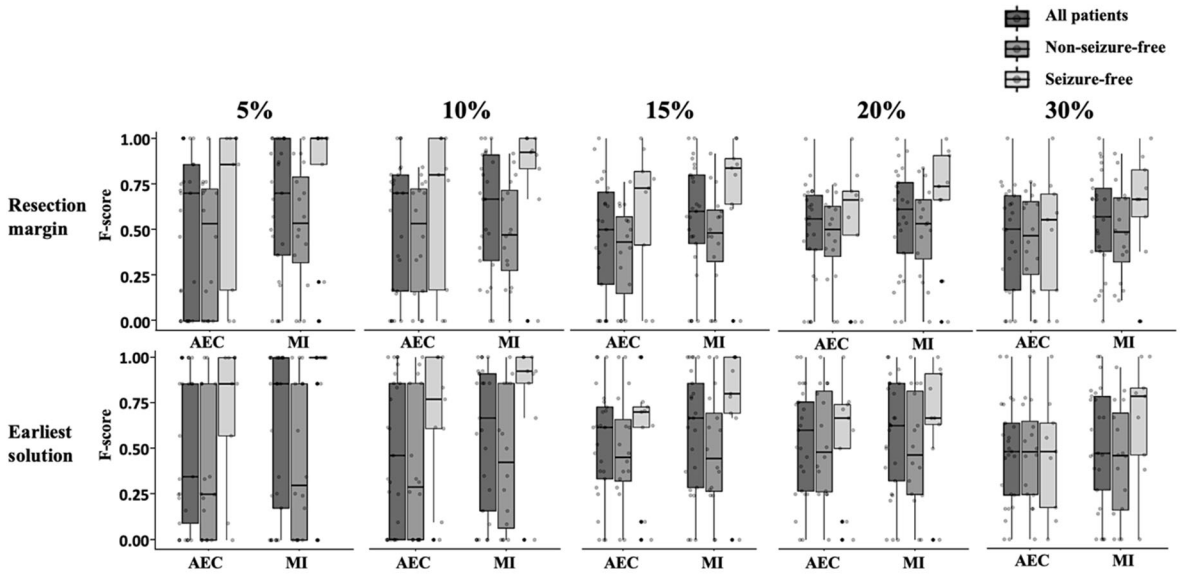

Supplementary Fig. 2. F-scores of AEC-VIZ and MI-VIZ in predicting the resection margin and the earliest solution using different thresholds to define the VIZ hotspot.

An additional four thresholds, 5%, 10%, 15% and 30%, were explored along with 20% threshold to define the VIZ hotspot through ranking all VIZ nodes by NI values. Although MI-VIZ achieve remarkable F-scores to predict the resection margin and the earliest solution, the top 5% and 10% thresholds do not fully represent the predictive power of the models, as too few VIZ nodes are defined as hotspot sources. For example, the MI-VIZ from Patient 1 Seizure 1 (Supplementary Fig. 4) has 34 VIZ nodes, which results in two and three hotspot nodes respectively if 5% and 10% thresholds are applied. When thresholds are over 10%, such as 15%, 20% and 30%, F-scores of AEC-VIZ and MI-VIZ are relatively similar. Although 15% threshold seems to offer the optimal predictive power among five thresholds we explored, in this paper we presented results from the top 20% threshold of VIZ nodes to be defined as hotspots to ensure that our work has the same thresholding strategy that was used by HDEEG and MEG source localisation in our previous publication [10]

.

Statistical analysis

First, we evaluated whether there is any association between VIZ hotspots and boundaries against the clinical localisation. Mixed-effects logistic regression modelling was used, with the outcome being resection margin, iEEG SOZ, early-MSL, mid-MSL, late-MSL, and the earliest solution (whether given by early-MSL or early-ESL). The variable in the modelling was a binary variable with 1 if a node was in VIZ hotspot or VIZ boundary and 0 if a node was not in VIZ hotspot or VIZ boundary. Results are expressed as odds ratios (OR) with 95% confidence interval (CI), p-values, Akaike Information Criterion (AIC) [22] and Bayesian Information Criterion (BIC) [23] (Supplementary Table 1, Supplementary Table 2).

	AEC-VIZ hotspot				**MI-VIZ hotspot**			
Outcome	**OR (95% CI)**	**AIC**	**BIC**	**P-value**	**OR (95% CI)**	**AIC**	**BIC**	**P-value**
Resection margin	4.701 (3.185, 6.595)	1825	1843.2	<0.001	7.232 (4.853, 10.56)	1773.5	1791.7	<0.001
iEEG SOZ	6.758 (3.225, 9.902)	599.1	617.4	<0.001	5.268 (2.101, 9.219)	615.4	633.6	<0.001
Earliest solution	4.158 (2.738, 6.147)	1451.1	1469.4	<0.001	5.658 (3.891, 8.139)	1431.7	1449.9	<0.001
Early-MSL	3.617 (2.4, 5.326)	1373.5	1391.8	<0.001	3.786 (2.495, 5.74)	1365.2	1383.4	<0.001
Mid-MSL	1.492 (0.644, 2.011)	1423.7	1441.9	0.061	1.847 (1.057, 2.927)	1427.3	1445.5	0.002
Late-MSL	1.08 (0.556, 1.917)	1216.8	1235.1	0.802	1.452 (0.797, 2.47)	1215.3	1233.5	0.185

Supplementary Table 1. Odds ratios (95% CI), AIC, BIC and p-values from mixed-effect logistic regression model of assessing statistical relationship between VIZ hotspot and clinical localisation (resection margin, iEEG SOZ, early-MSL, mid-MSL, late-MSL, and the earliest solution).

	AEC-VIZ boundary				**MI-VIZ boundary**			
Outcome	**OR (95% CI)**	**AIC**	**BIC**	**P-value**	**OR (95% CI)**	**AIC**	**BIC**	**P-value**
Resection margin	2.52 (2.02, 3.14)	2261.8	2280.2	<0.001	4.67 (3.70, 5.91)	2151.6	2170	<0.001
iEEG SOZ	3.04 (1.95, 4.75)	648.55	664.66	<0.001	3.74 (2.37, 5.89)	639.5	655.6	<0.001
Earliest solution	3.22 (2.47, 4.18)	1784.5	1802.9	<0.001	3.51 (2.70, 4.57)	1729.9	1748.3	<0.001
Early-MSL	1.42 (1.06, 1.91)	1734.67	1753.1	<0.001	1.59 (1.18, 2.13)	1723	1741.4	<0.001
Mid-MSL	1.11 (0.81, 1.54)	1482.9	1501.3	0.02	1.44 (1.04, 1.98)	1479.2	1479.6	0.002
Late-MSL	3.19 (2.46, 4.13)	1314	1332.4	0.518	4.61 (3.53, 6.03)	1309.6	1328	0.027

Supplementary Table 2. Odds ratios (95% CI), AIC, BIC and p-values from mixed-effect logistic regression model of assessing statistical relationship between VIZ boundary and clinical localisation (resection margin, iEEG SOZ, early-MSL, mid-MSL, late-MSL, and the earliest solution).

Next, we calculated precision (or positive predictive values) and recall (or sensitivity) of VIZ hotspot and VIZ boundary for predicting the resection margin and clinical localisation. The precision of VIZ hotspot and recall of VIZ boundary were used to compute F-scores to assess the performance of our proposed model in predicting the clinical localisation. Supplementary Fig. 3 demonstrates the precision and recall of VIZ (hotspot and boundary) in predicting the resection margin and the earliest solution when the top 20% VIZ nodes ranked by NI values are defined as the VIZ hotspot.

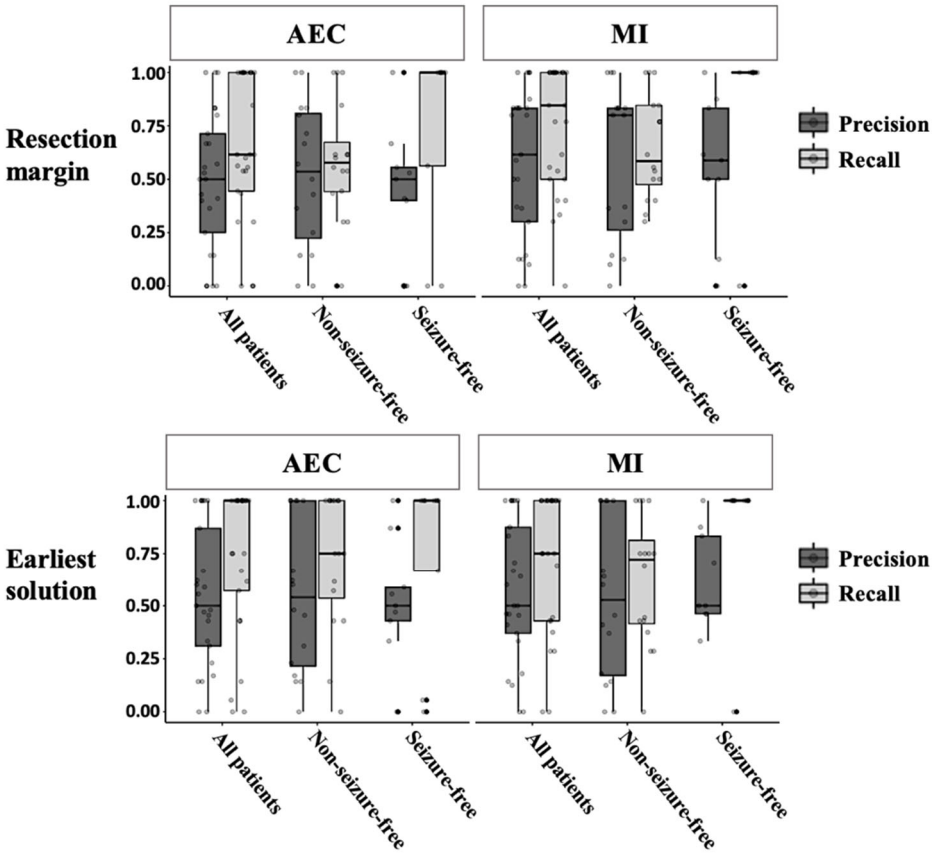

Supplementary Figure 3. VIZ hotspot precision and VIZ boundary recall in predicting the resection margin (above) and the earliest solution (below). The hotspot is defined as the top 20% VIZ nodes ranked by NI values.

Supplementary Fig. 3 shows that the MI-VIZ recall (for VIZ boundary) sufficiently captures the entirety of resection margin and the earliest solution and identifies non-ictogenic brain areas that are less likely to overlap with the EZ and are therefore potentially less concerning for iEEG coverage. Moderate precision values (for VIZ hotspot) are found for both AEC-VIZ and MI-VIZ in predicting the resection margin and earliest solution. MI-VIZ hotspots appear

to have higher precision than AEC-VIZ hotspots in predicting the resection margin and, to a lesser degree, the earliest solution. The spatial overlap between VIZ and clinical localisation are demonstrated on a per patient and per seizure basis in Supplementary Table 3.

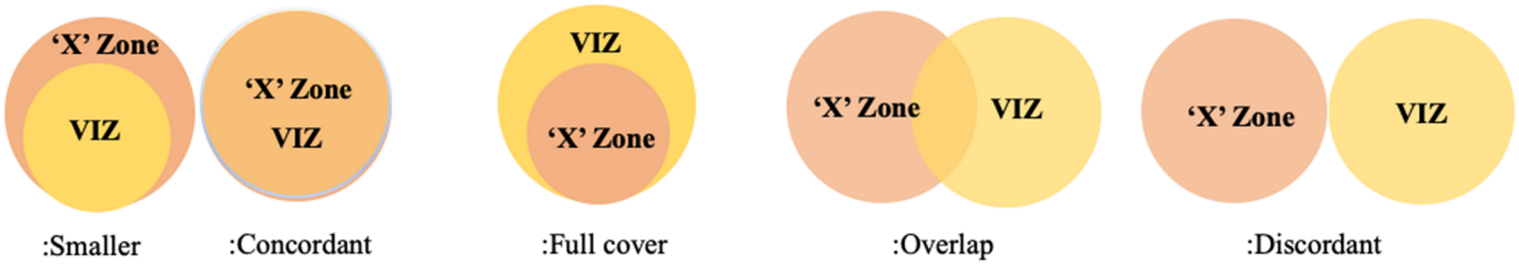

'X' zone	Outcome	Patient	seizure		Patient	seizure		Patient	seizure		Patient	seizure	
			AEC	MI		AEC	MI		AEC	MI		AEC	MI
Resection margin	Seizure-free	-/6	-/9	-/9	4	6	8	1	1	0	1	2	1
	Non-seizure-free	-/6	-/16	-/16	1	2	2	4	8	10	1	6	4
iEEG SOZ		-/2	-/3	-/3	1	1	3	1	1	-	-	1	-
		-/4	-/8	-/8	2	3	3	1	1	1	1	4	4
Earliest solution		-/6	-/9	-/9	4	6	8	1	1	-	1	2	1
		-/6	-/16	-/16	2	5	4	2	5	6	2	6	6
Early-MSL		-/6	-/9	-/9	3	4	6	1	1	-	2	4	3
		-/6	-/16	-/16	2	4	4	2	5	6	2	7	6
Mid, late - MSL		-/6	-/9	-/9	2	2	2	-	-	-	4	7	7
		-/6	-/16	-/16	1	5	5	2	3	3	3	8	8

Supplementary Table 3. Per-patient and per-seizure concordance between VIZ (AEC and MI) and clinical localisation. The five categories of concordance (at top) are based on spatial overlap relations between the VIZ boundary (VIZ) and clinical localisation ('X' zone), and are given as smaller VIZ, concordant, VIZ fully covers X zone, VIZ and X zone overlap, discordant. X zones (at left) are given as resection margin, iEEG SOZ, MSL solutions (early-, mid-, late-MSL) and the earliest source localisation solution. Patients and seizures are grouped based on surgical outcome (seizure-free or non-seizure-free). No VIZ boundary is found to be smaller or completely concordant with any X zone.

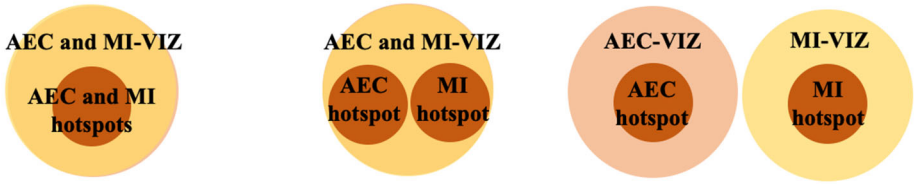

Outcome	Boundary concordant with the same 'hotspot'/seizure	Boundary concordant with the different 'hotspot'/seizure	Boundary discordant
Seizure-free	7/9	-	2
Non-seizure-free	9/16	1	6

Supplementary Table 4. Spatial overlap between respective hotspots and boundaries for AEC-VIZ and MI-VIZ . Seizure counts are grouped based on surgical outcomes (seizure-free and non-seizure-free). 16/25 seizures have AEC-VIZ hotspot and boundary concordance with MI-VIZ, while 9 seizures have AEC-VIZ with a different hotspot from MI-VIZ, with the majority of these (8/9 seizures) discordant for the VIZ boundary as well.

It is also worth noting that AEC-VIZ and MI-VIZ do not always present concordant hotspots or boundaries. As shown in Supplementary Table 4, 16/25 seizures show AEC-VIZ and MI-VIZ concordance for both hotspot and boundary, 9/25 seizures show AEC-VIZ and MI-VIZ discordance for hotspot, with the majority of these patients experiencing seizure recurrence post-operatively. Thus, discordance of AEC-VIZ and MI-VIZ hotspots may offer complementary information and additional insights to alternative surgical strategies for non-seizure-free patients.

Notes: NDS for non-disabling seizure; DS for disabling seizures; FC for Full Cover; PO for Partial Overlap; NO for No Overlap; VIZ for virtual ictogenic zone; iEEG SOZ for iEEG seizure onset zone; MSL is magnetoencephalographic source localisations. CD for cortical dysplasia. *Only iEEG report available for patient 7 and 9.

Patient ID	MRI	Histology	Surgical outcome	VIZ vs Resection margin			VIZ vs iEEG SOZ			VIZ vs Early-MSL			VIZ vs Earliest solution			
				Seizure	AEC	MI	Seizure	AEC	MI	Seizure	AEC	MI	Earliest solution	Seizure	AEC	MI
1	Normal	CD 1A	Engel class I Rare NDS	1	PO	PO	1	PO	PO	1	FC	PO	Early-MSL	1	FC	PO
2	Normal	CD 1	Engel class I Seizure free	1	FC	FC	iEEG is not done			1	FC	FC	Early-ESL	1	FC	FC
				2	FC	FC				2	FC	FC		2	FC	FC
3	Normal	CD 2A	Engel class I Rare NDS	1	PO	PO	iEEG is not done			1	PO	PO	Early-MSL	1	PO	PO
				2	PO	PO				2	PO	PO		2	PO	PO
				3	PO	PO				3	PO	PO		3	PO	PO
				4	PO	PO				4	PO	PO		4	PO	PO
				5	NO	PO				5	FC	FC		5	FC	FC
				6	PO	PO				6	PO	PO		6	PO	PO
4	Normal	Non-specific	Engel class III Fewer DS	1	NO	NO	1	NO	NO	1	NO	NO	Early-MSL	1	NO	NO
				2	NO	NO	2	NO	NO	2	NO	NO		2	NO	NO
				3	NO	NO	3	PO	PO	3	NO	NO		3	NO	NO
				4	FC	FC	4	FC	FC	4	NO	NO		4	NO	NO
				5	NO	NO	5	NO	NO	5	NO	NO		5	NO	NO
5	Normal	CD 1C	Engel class I Seizure free	1	FC	FC	1	FC	FC	1	FC	FC	Early-MSL	1	FC	FC
6	Normal	CD 2A	Engel class I Seizure free	1	FC	FC	iEEG is not done			1	FC	FC	Early-ESL	1	FC	FC
7	Normal	CD 2A	Engel class I Seizure free	1	NO	NO	Only iEEG report available*			1	NO	NO	Non-localising	1	NO	NO
8	Normal	CD 1	Engel class I Seizure free	1	FC	FC	iEEG is not done			1	NO	NO	Early-ESL	1	FC	FC
				2	FC	FC				2	NO	NO		2	FC	FC

257
258

Patient ID	MRI	Histology	Surgical outcome	VIZ vs Resection margin			VIZ vs iEEG SOZ			VIZ vs Early-MSL			VIZ vs Earliest solution			
				Seizure	**AEC**	**MI**	**Seizure**	**AEC**	**MI**	**Seizure**	**AEC**	**MI**	**Earliest solution**	**Seizure**	**AEC**	**MI**
9	Normal	CD 2B	Engel class II Rare DS	1	PO	PO	Only iEEG report available*			1	NO	NO	Early-ESL	1	NO	NO
10	Multi-lobar dysplasia	Normal	Engel class I NDS only	1	FC	FC	1	FC	FC	1	FC	FC	Early-MSL	1	FC	FC
11	Multi-lobar dysplasia	Ischemia	Engel class III Fewer DS	1	NO	PO	1	FC	FC	1	FC	FC	Early-MSL	1	FC	FC
				2	PO	PO	2	FC	FC	2	FC	FC		2	FC	FC
12	Right frontal gliosis	Gliosis	Engel class I Seizure free	1	PO	FC	1	PO	FC	1	PO	FC	Early-ESL	1	PO	FC
				2	NO	FC	2	NO	FC	2	NO	FC		2	NO	FC

Notes: NDS for non-disabling seizure; DS for disabling seizures; FC for Full Cover; PO for Partial Overlap; NO for No Overlap; VIZ for virtual ictogenic zone; iEEG SOZ for iEEG seizure onset zone; MSL is magnetoencephalographic source localisations. CD for cortical dysplasia.

*Only iEEG report available for patient 7 and 9.

259 260 261 262 263 264 265 266 267 268 269 270 271 272 273 274 275 276 277 278 279

Supplementary Table 5. Patient data and overlap with VIZ results for all seizures.

Abbreviations: CD (Cortical Dysplasia), PO (partial overlap), FC (full cover), NO (no overlap).

Results summary (also refer to Supplementary Table 5)

Patient 1

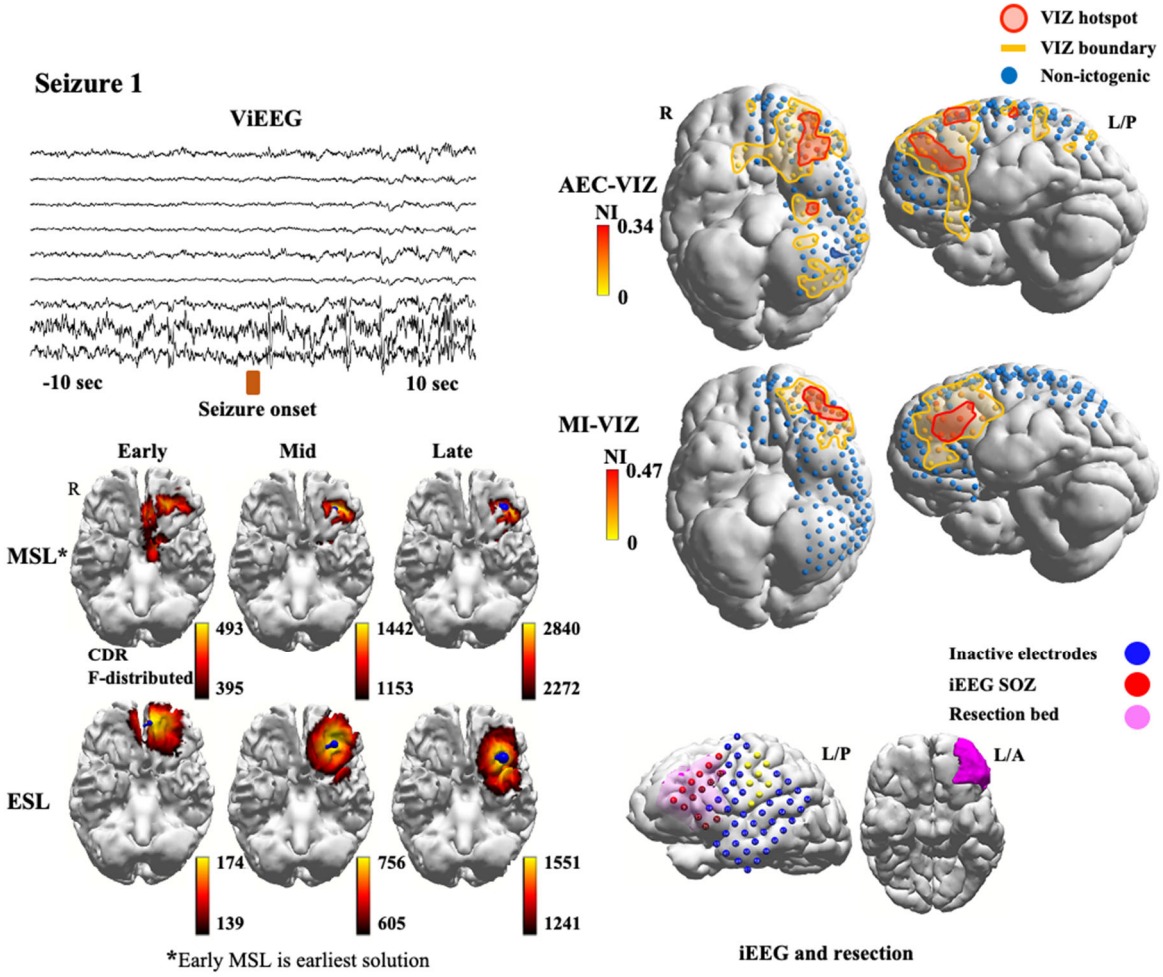

Supplementary Figure 4. Patient 1 had a normal MRI with over 10 disabling seizures per month before surgery. The patient had five disabling seizures when medication was adjusted but is now seizure-free again at month 39. MEG sLORETA ictal early source localisation suggested a focus at the left medial orbitofrontal gyrus and rectal gyrus. Guided by MSL solutions, ViEEGs were defined to extensively cover the left orbitofrontal, lateral frontal, and temporo-parietal areas. Source signals of six seizure events were reconstructed but only the first seizure gave a distinct morphology for ictal spikes. AEC-VIZ and MI-VIZ identified hotspot (nodes in red line and shade) encompassing two isolated islands: one in the orbitofrontal and the other in dorsolateral frontal convexity. The orbitofrontal component of AEC-VIZ and MI-VIZ best overlap the MSL sLORETA solutions and partially overlap the surgical resection bed. This patient has achieved Engel I outcome with rare non-disabling seizures. Based on the surgical outcome, the MEG derived AEC-VIZ and MI-VIZ results suggest another epileptic focus outside the current resection volume.

Patient 2

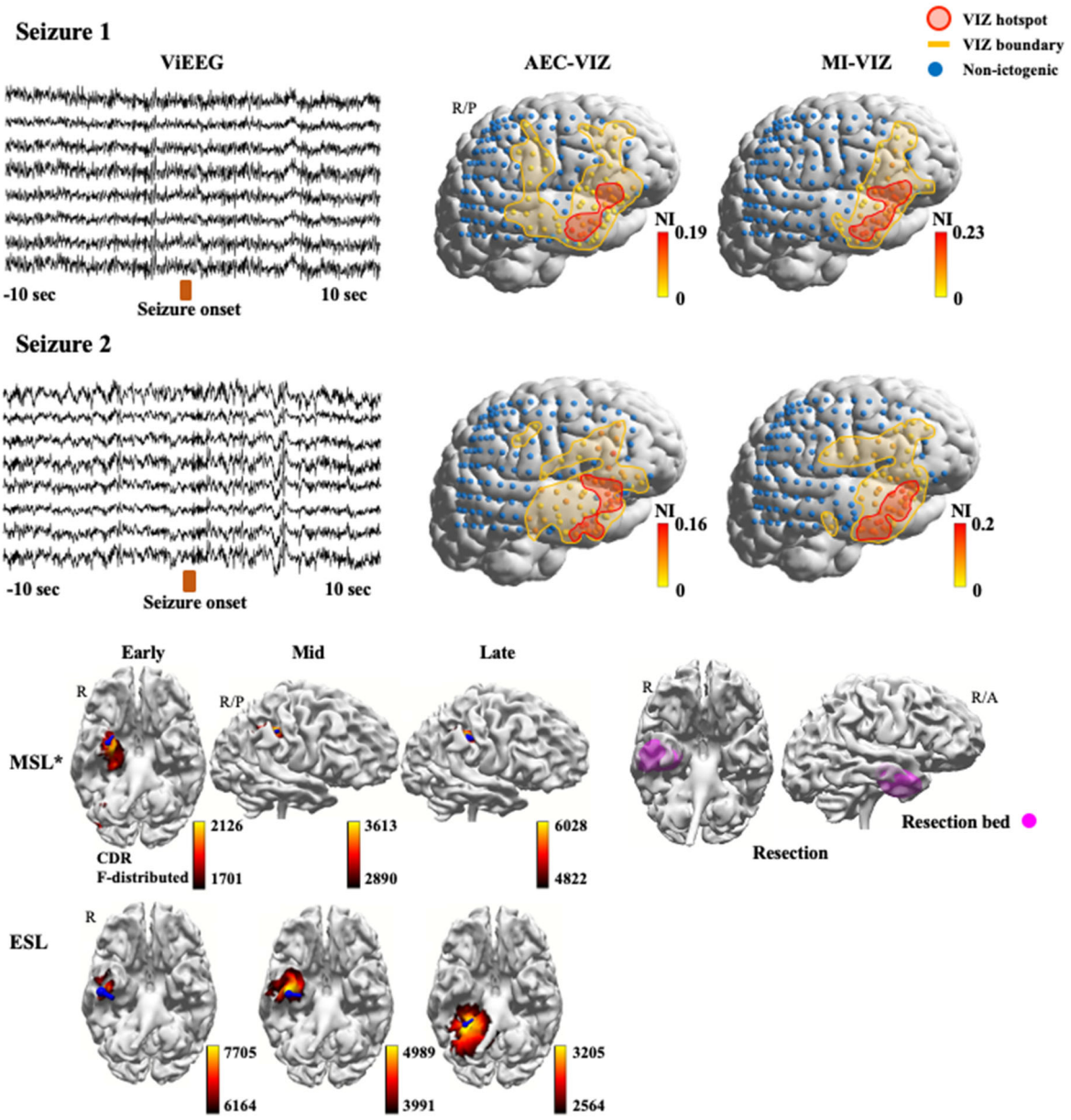

Supplementary Figure 5. Patient 2 had a normal MRI with an average of 5 seizures per month before surgery and is seizure free at 26 months follow-up. MEG sLORETA ictal early source localisation suggested a focus at right temporal pole. Guided by MSL solutions, ViEEG was defined to extensively cover the right temporal pole, lateral temporal, parietal, and lateral frontal areas. Source signals of two MEG captured seizure events are reconstructed. Ictal discharges can be seen in the representative ViEEG channels. Both AEC-VIZ and MI-VIZ identified hotspots (nodes in red line and shade) over the right lateral temporal pole. Note the overlap with the early MSL solution and the surgical resection and the lack of overlap with the ESL solutions, which were more postero-basal in location. This patient

has achieved an Engel I seizure-free outcome. Both the AEC-VIZ and MI-VIZ successfully captured the EZ.

Patient 3

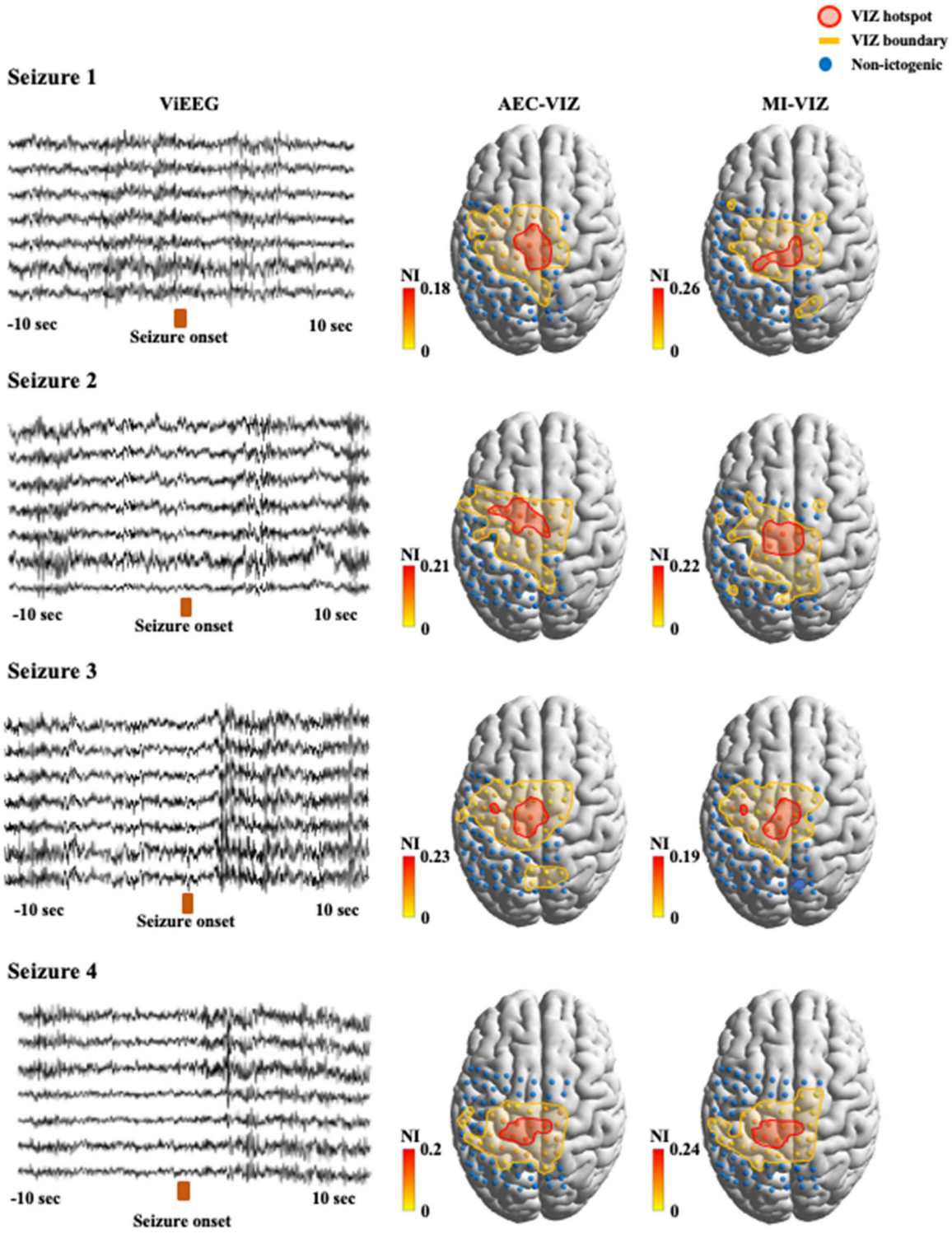
VIZ hotspot
VIZ boundary
Non-ictogenic
Seizure 1
ViEEG
AEC-VIZ
MI-VIZ
-10 sec
Seizure onset
10 sec
NI
0.18
0
NI
0.26
0
Seizure 2
-10 sec
Seizure onset
10 sec
NI
0.21
0
NI
0.22
0
Seizure 3
-10 sec
Seizure onset
10 sec
NI
0.23
0
NI
0.19
0
Seizure 4
-10 sec
Seizure onset
10 sec
NI
0.2
0
NI
0.24
0

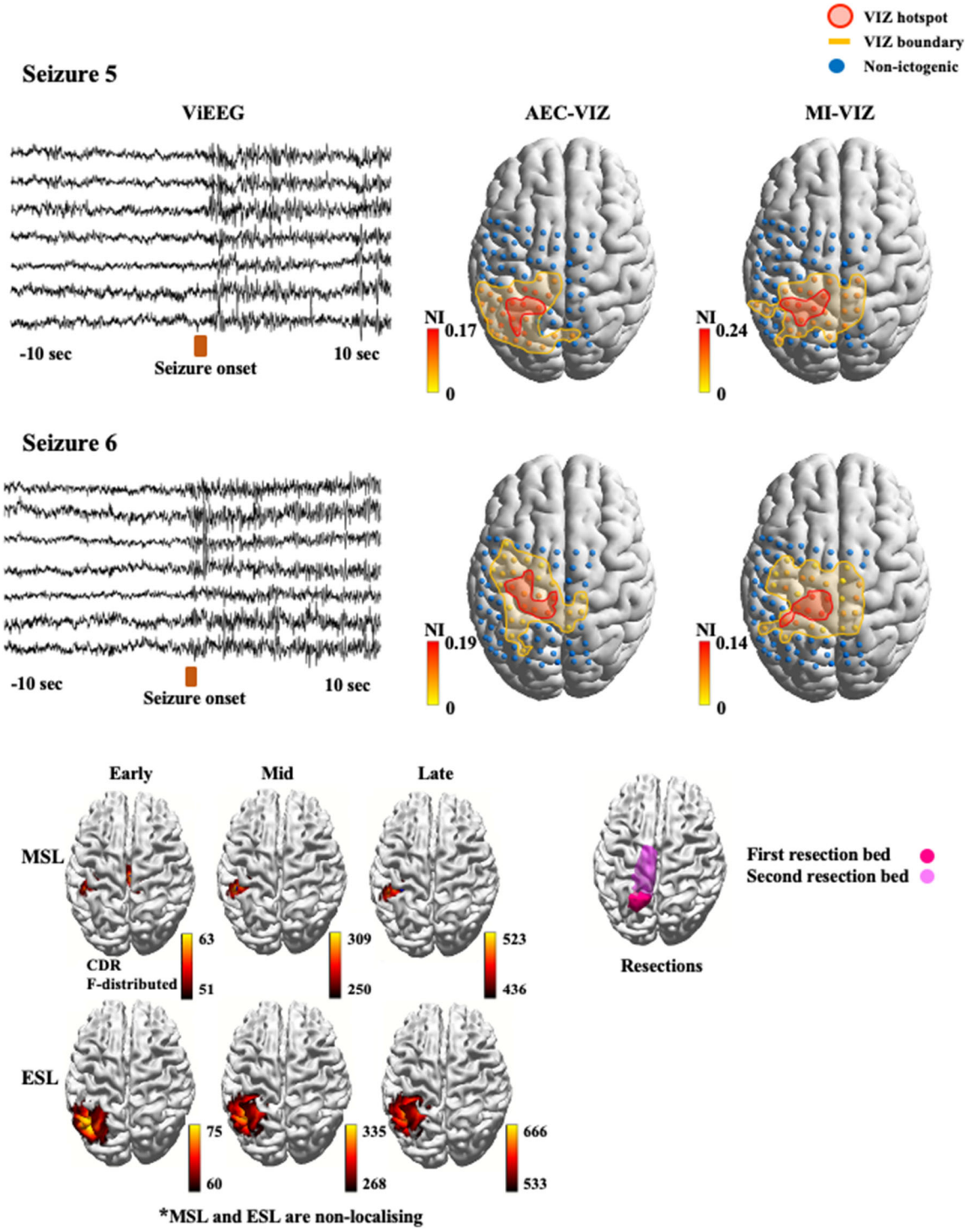

Supplementary Figure 6. Patient 3 had a normal MRI with over 100 seizure events per month before surgery and infrequent non-disabling seizures at 23 months post-surgery (Engel I). MEG sLORETA ictal early source localisation suggested a focus at the left paracentral lobule. Guided by MSL solutions, ViEEGs were defined to extensively cover vertex, left parietal, and lateral temporal areas. Source signals of seven MEG captured seizure events are reconstructed while six seizures present

distinct morphology of ictal spikes. Ictal discharges can be seen in the representative ViEEG channels with a spatial distribution that is similar across the seizure events. Both AEC-VIZ and MI-VIZ identified hotspots (nodes in red line and shade) encompassing the left paracentral lobule. This area is highlighted by five seizures (Seizure 1, Seizure 2, Seizure 3, Seizure 4, Seizure 6). AEC-VIZ derived from Seizure 5 spreads laterally while MI-VIZ extends medially. Therefore, both AEC-VIZ and MI-VIZ from MEG data better concord with the earliest solution given by MSL. This patient has achieved Engel I outcome with rare non-disabling seizures. Based on the surgical outcome, the MEG derived AEC-VIZ and MI-VIZ successfully captured the bulk of the EZ.

Patient 4

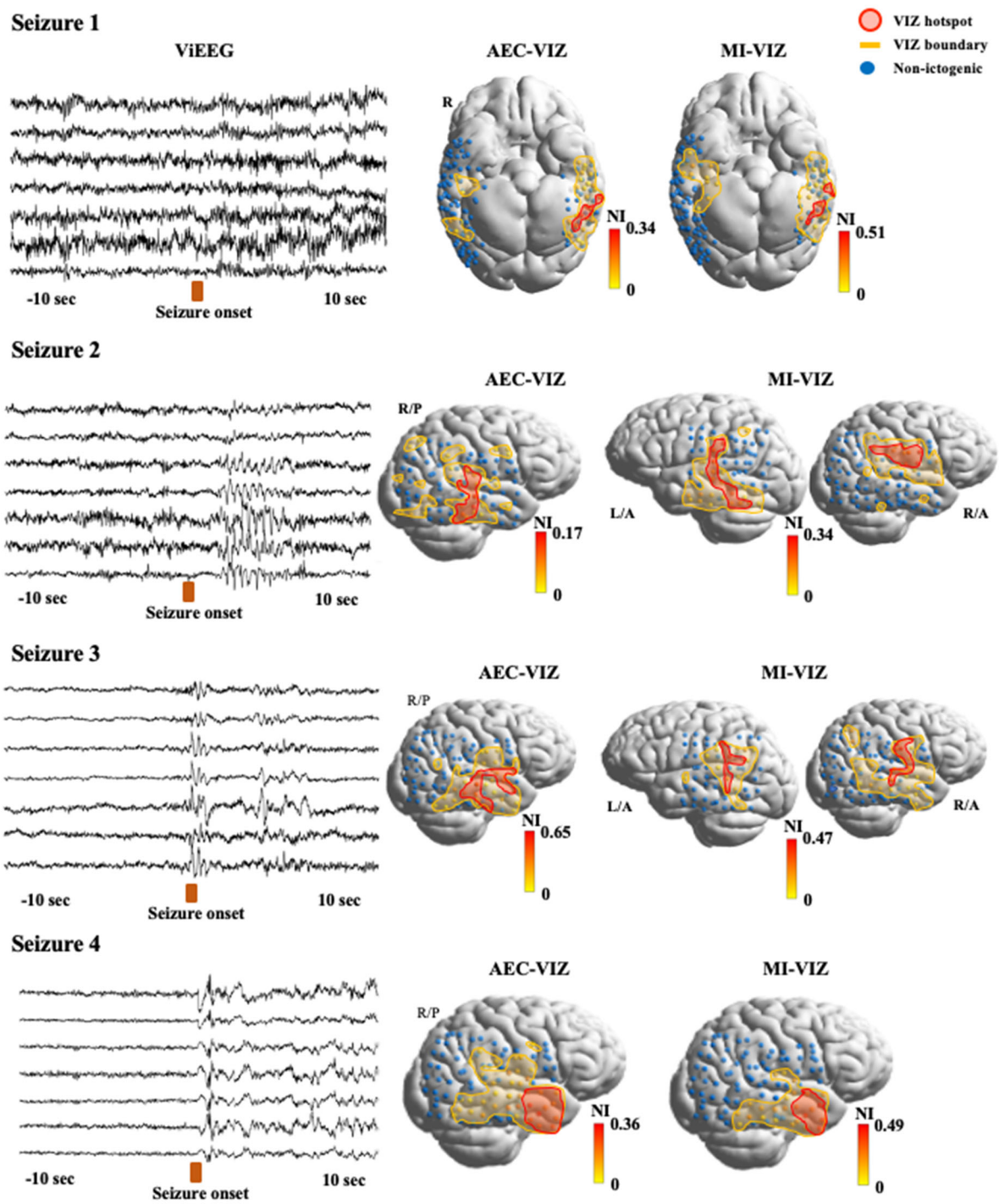
Seizure 1
ViEEG
AEC-VIZ
MI-VIZ
VIZ hotspot
VIZ boundary
Non-ictogenic
R
NI 0.34
0
NI 0.51
0
-10 sec
Seizure onset
10 sec
Seizure 2
AEC-VIZ
MI-VIZ
R/P
NI 0.17
0
L/A
R/A
NI 0.34
0
-10 sec
Seizure onset
10 sec
Seizure 3
AEC-VIZ
MI-VIZ
R/P
NI 0.65
0
L/A
R/A
NI 0.47
0
-10 sec
Seizure onset
10 sec
Seizure 4
AEC-VIZ
MI-VIZ
R/P
NI 0.36
0
NI 0.49
0
-10 sec
Seizure onset
10 sec

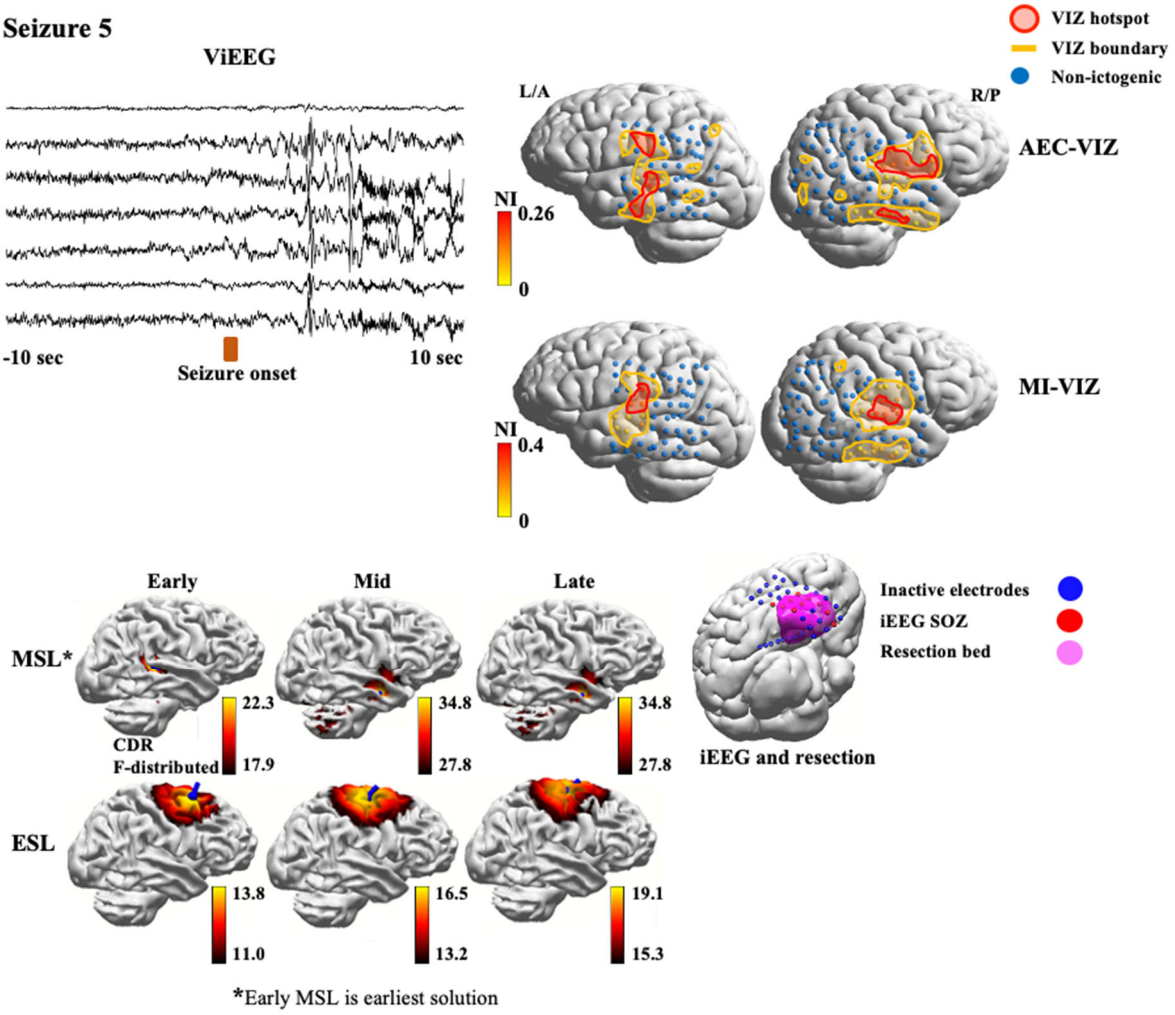

Supplementary Figure 7. Patient 4 had a normal MRI with over 20 seizure events per month before surgery. After surgery, the patient had infrequent disabling and non-disabling seizures at 21 months follow-up. MEG sLORETA ictal early source localisation suggested a focus at the posterior superior temporal gyrus. Guided by MSL solutions, ViEEGs were defined to extensively cover bilateral temporal, parietal, and occipital areas in a non-regularized pattern to enhance detection of VIZ beyond regular iEEG configurations. Source signals of eight MEG captured seizure events are reconstructed while five seizures present distinct morphology of ictal spikes. Ictal discharges can be seen in the representative ViEEG channels. AEC-VIZ and MI-VIZ identified different hotspots using Seizure 2, Seizure 3, and Seizure 5, while AEC-VIZ and MI-VIZ hotspots agree in Seizure 1 and Seizure 4. Variability of AEC-VIZ and MI-VIZ boundaries is observed between seizures; multiple, bilateral regions are identified to be VIZ hotspots (high NI values). This patient has achieved Engel III outcome with fewer disabling seizures. Based on the suboptimal surgical outcome, the MEG derived AEC-VIZ and MI-VIZ may suggest epileptic foci outside the current resection.

Patient 5

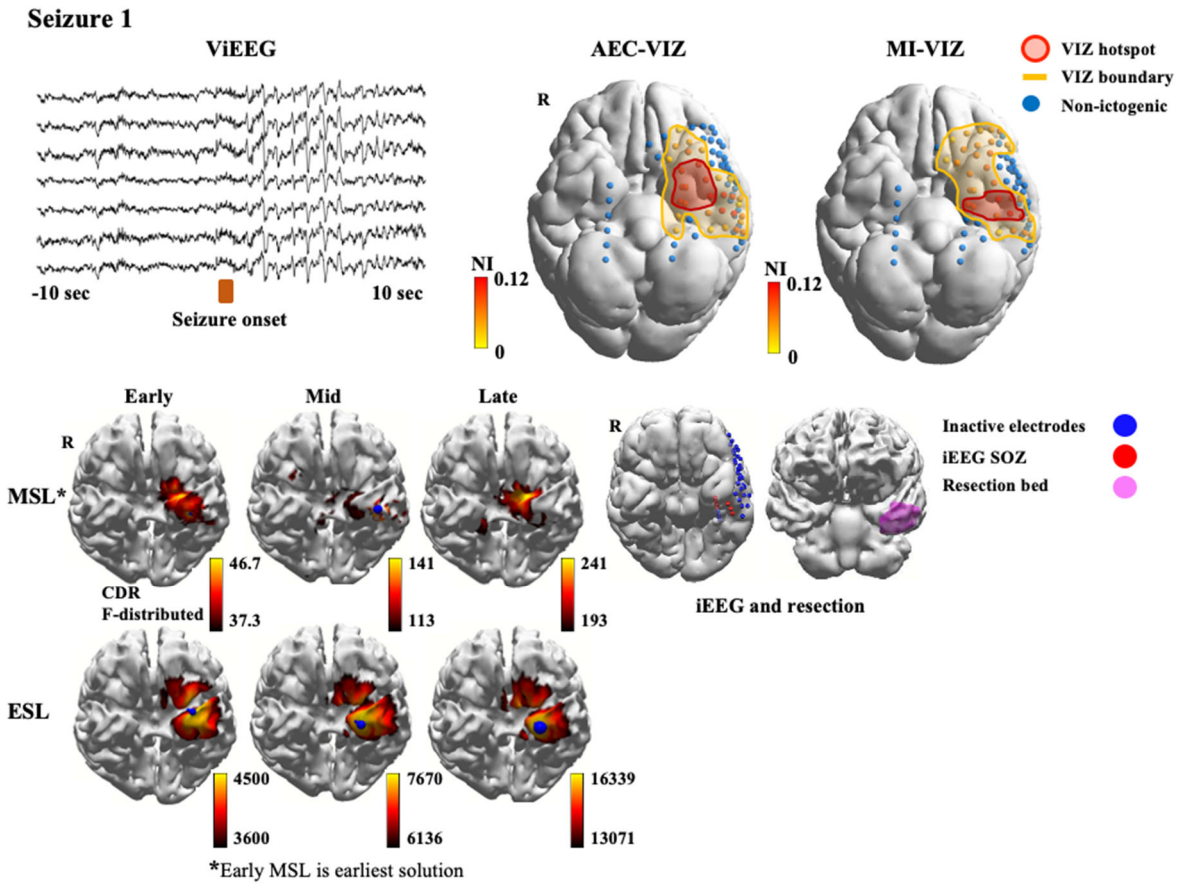

Supplementary Figure 8. Patient 5 had a normal MRI with over 20 seizures per month before surgery and is seizure free at 20 months follow-up. MEG sLORETA ictal source localisation suggested a focus at the mesial temporal region before propagation to the temporal pole. Guided by MSL solutions, ViEEGs were defined to extensively cover basal, inferior and lateral temporal areas. Two depth electrode-like ViEEGs were also defined to cover both hippocampi. Source signals of two MEG captured seizures are reconstructed while only the first seizure presents distinct morphology for ictal spikes. Ictal discharges can be seen in the representative ViEEG channels. Both AEC-VIZ and MI-VIZ identified hotspots (nodes in red line and shade) encompassing the left mesio-basal temporal region. AEC-VIZ and MI-VIZ hotspots concord with both MSL and ESL solutions. However, the extent of both AEC-VIZ and MI-VIZ are broader than resection margins and MSL solutions. This patient has achieved Engel I seizure-free outcome. Based on the seizure-free outcome, the MEG derived AEC-VIZ and MI-VIZ successfully captured the EZ.

Patient 6

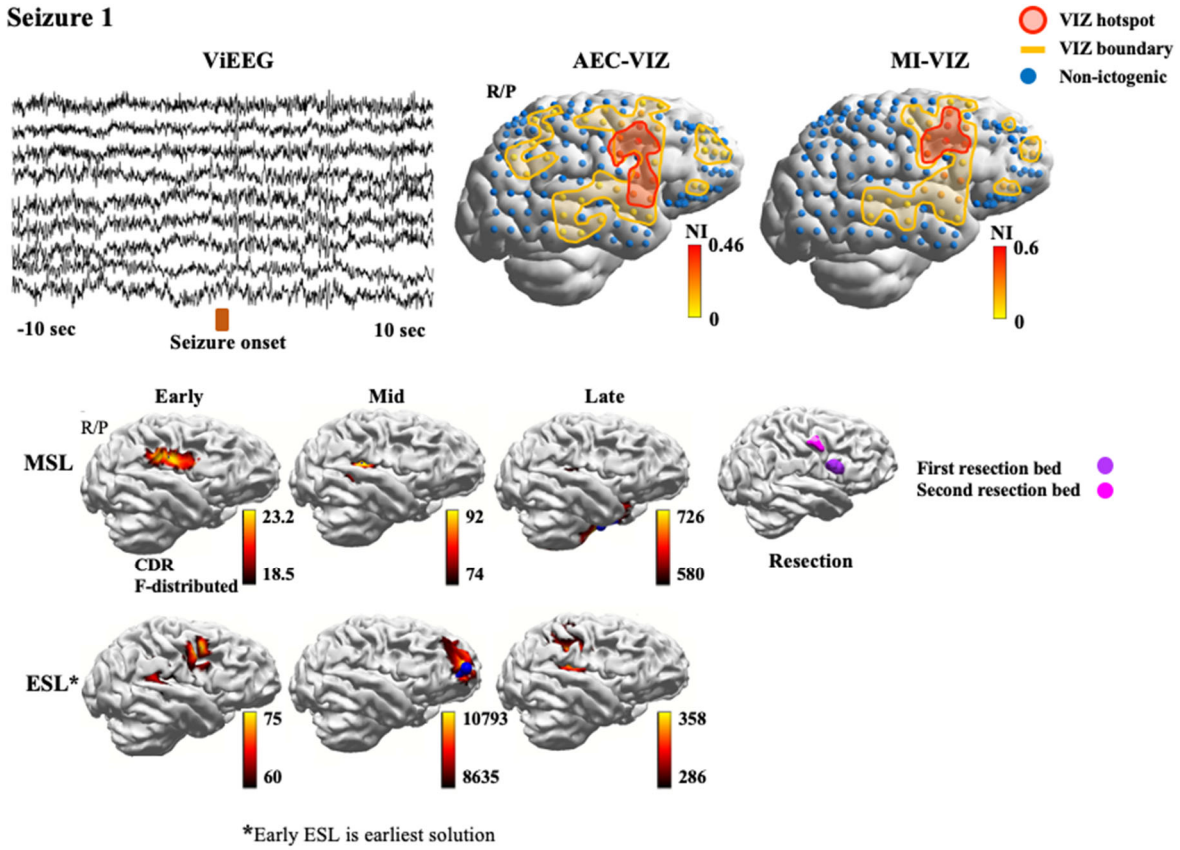

Supplementary Figure 9. Patient 6 had a normal MRI with over 100 seizures per month before surgery, which led to an Engel I outcome. MEG and EEG sLORETA ictal early source localisation suggested a focus in the region of the right central sulcus and pre-motor cortex. Guided by MSL solutions, ViEEGs were defined to extensively cover lateral parietal, temporal, and frontal areas including the frontal pole. Source signals of MEG captured continuous spikes are reconstructed. Continuous spikes can be seen in the representative ViEEG channels. AEC-VIZ and MI-VIZ identified hotspots (nodes in red line and shade) encompassing a focus at the right pre-motor cortex. Note the overlap with the early ESL solution and the surgical resection and the lack of overlap with the MSL solutions. Hence, AEC-VIZ and MI-VIZ from MEG data better concords with the earliest solution given by the EEG rather than the corresponding MEG sLORETA solution. This patient has achieved Engel I seizure-free outcome according to the latest review (over two years since surgery that showed a cortical dysplasia). Based on the surgical outcome, the MEG derived AEC-VIZ and MI-VIZ successfully captured the EZ, while the MEG derived sLORETA solution did not.

Patient 7

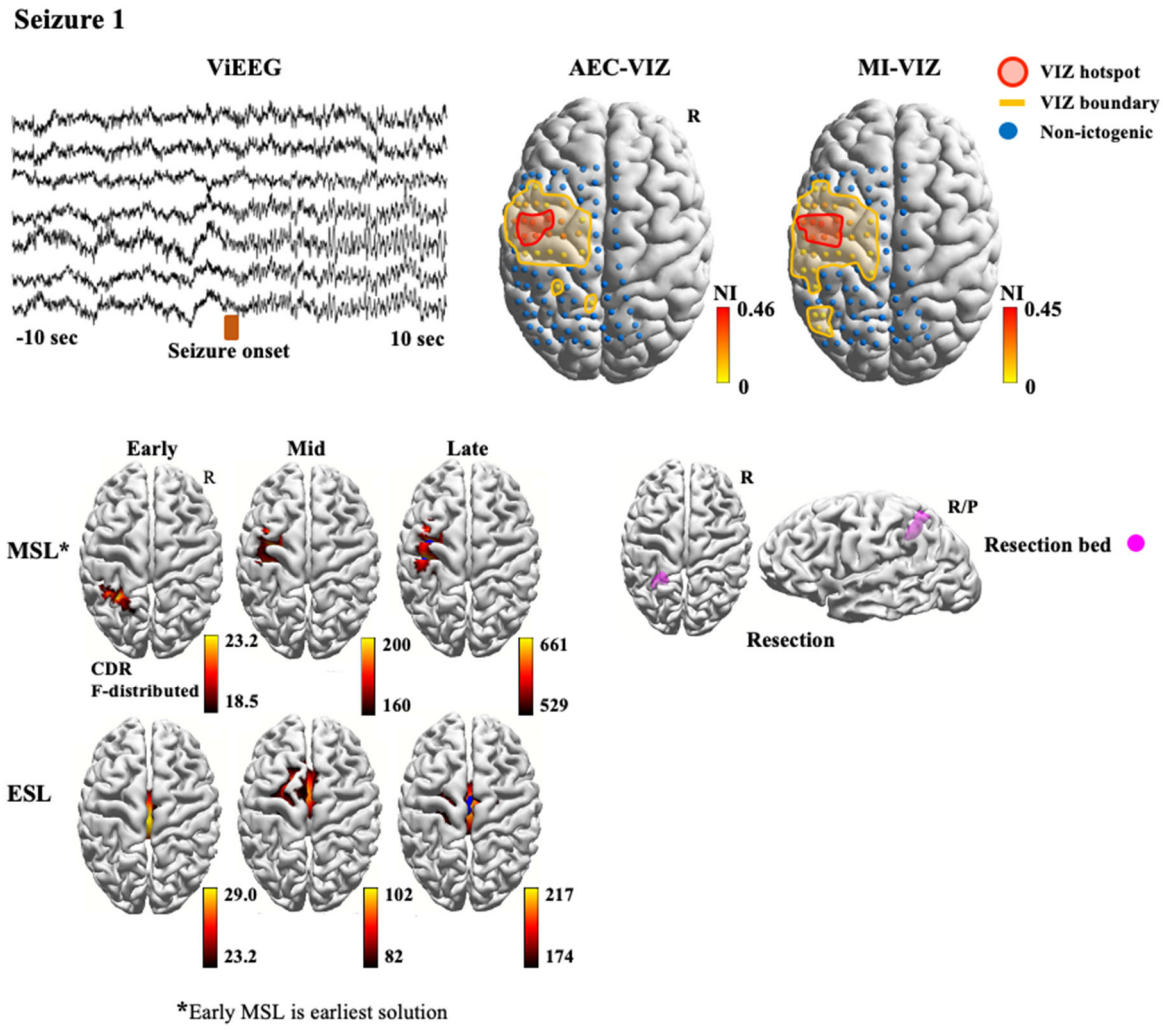

Supplementary Figure 10. Patient 7 had a normal MRI with over 100 seizures per month before surgery and is seizure-free at 20 months follow-up. EEG and MEG sLORETA source localisation of ictal discharges was non-localising while MEG sLORETA early source localisation of interictal discharges suggested a focus at the junction of post-central sulcus and superior parietal lobule (ESL and MSL solutions using interictal spikes shown). Guided by MSL solutions using interictal spikes, ViEEGs were defined to extensively cover frontal, parietal and anterior occipital areas. Source signals of a MEG captured seizure is reconstructed. Ictal discharges can be seen in the representative ViEEG channels. Both AEC and MI-VIZ identified hotspots (nodes in red line and shade) encompassing a localised area of the left central sulcus extending laterally. AEC-VIZ and MI-VIZ do not overlap the early-MSL (interictal) nor the surgical resection but better concords with mid-MSL (interictal) and late-MSL (interictal).This patient has achieved Engel I seizure-free outcome (histology was cortical

388 dysplasia). Based on the seizure free outcome, the MEG derived AEC and MI-VIZ did not capture the
389 EZ.

Patient 8

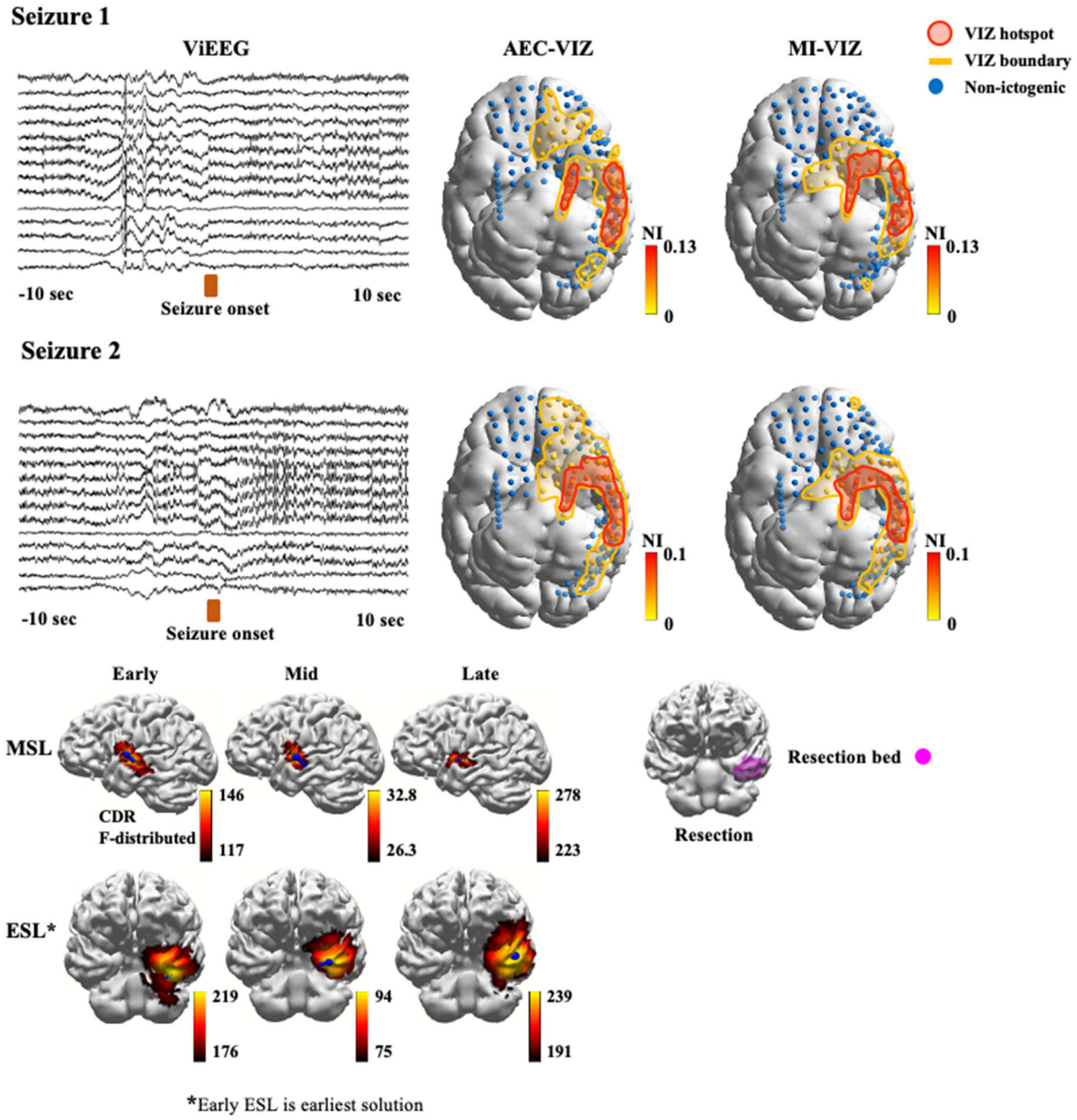

Supplementary Figure 11. Patient 8 had a normal MRI with over 20 seizures per month before surgery and is seizure free at 22 months follow-up. MEG sLORETA ictal early source localisation suggested a focus at the left superior temporal gyrus. Based on this, ViEEGs were defined to extensively cover left lateral temporal, basal temporal, temporal pole, orbitofrontal, and frontal pole surfaces. Source signals of two MEG captured seizure events are reconstructed. Ictal discharges can be seen in the representative ViEEG channels with a spatial distribution that is similar across the two seizure events. Both AEC-VIZ and MI-VIZ identified hotspot (nodes in red line and shade) encompassing the left basal and mesial temporal structures including anterior hippocampus and temporal pole. Note the overlap with the ESL solutions and the surgical resection and the lack of

overlap with the MSL solutions. Hence, AEC-VIZ and MI-VIZ from MEG data better concords with the earliest solution given by the EEG rather than the corresponding MEG sLORETA solution. This patient has achieved Engel I seizure-free outcome according to the latest review (cortical dysplasia on histology). Based on the seizure free outcome, the MEG derived AEC-VIZ and MI-VIZ successfully captured the EZ while the MEG derived sLORETA solution, that sat well outside the resection bed, did not.

Patient 9

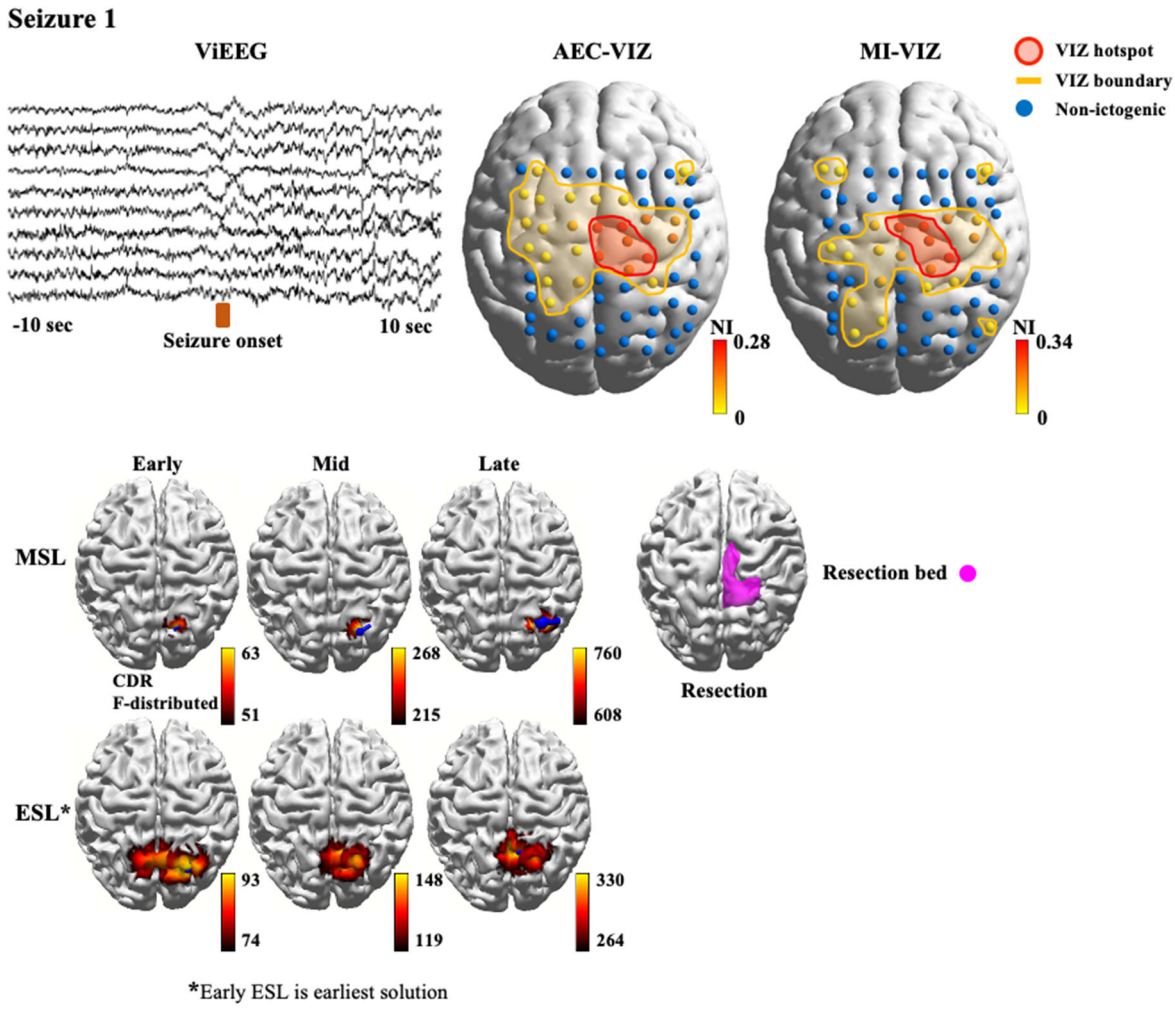

Supplementary Figure 12. Patient 9 had a normal MRI with over 100 seizures per month (motor left leg) before surgery. After surgery, the patient was seizure free for 6 months but then developed new left arm motor events. MEG sLORETA ictal early source localisation suggested a focus at the right posterior paracentral lobule and precuneus. Guided by MSL solutions, ViEEGs were defined to extensively cover the vertex, biparietal and posterior bifrontal areas. Source signals of two MEG captured seizures are reconstructed while only the first seizure presents a distinct morphology for ictal spikes. Ictal discharges can be seen in the representative ViEEG channels. Both AEC and MI-VIZ identified hotspots (nodes in red line and shade) encompassing the right paracentral lobule which does not concord with MSL or ESL solutions. This patient has achieved Engel II outcome with rare disabling seizures. The MEG derived AEC-VIZ and MI-VIZ overlap the surgical resection (that showed cortical dysplasia) but the return of seizures suggests that the EZ was not sufficiently removed.

Patient 10

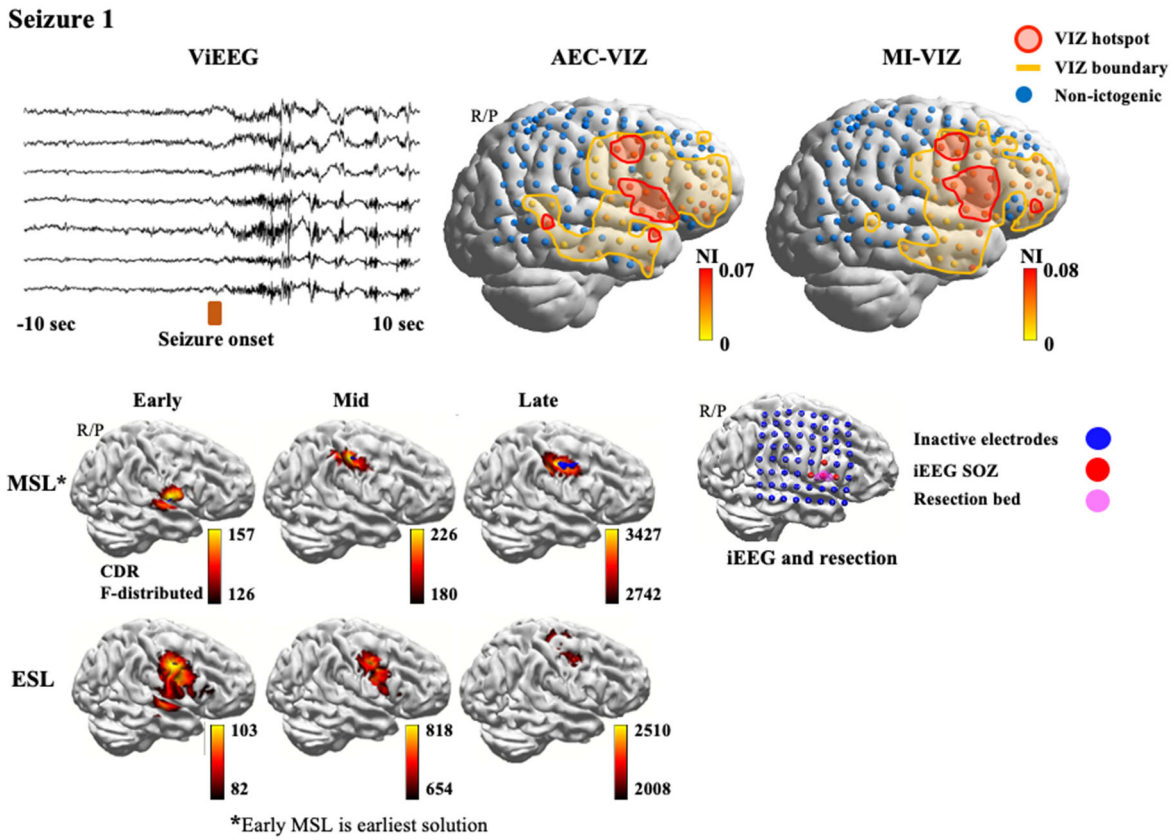

Supplementary Figure 13. Patient 10 had an extensive cortical dysplasia of the right fronto-temporo-parietal area with over 100 seizures per month before surgery, which was successful in stopping her disabling events. MEG sLORETA ictal early source localisation suggested a focus at the base of the pre-central gyrus. Guided by MSL solutions and by the extent of the dysplasia, ViEEGs were defined to extensively cover much of the right hemisphere. Source signals of MEG captured continuous spikes that are reconstructed and shown in the representative ViEEG channels. Both AEC-VIZ and MI-VIZ identified hotspots (nodes in red line and shade) containing two isolated areas (one inferior and the other superior) at the lateral frontal convexity where the inferior hotspot better concords with the resection margin, iEEG SOZ and the earliest solution given by MEG while the superior hotspot overlaps with the late-MSL and late-ESL. This patient has achieved Engel I outcome with non-disabling seizures. Based on surgical outcome, the MEG derived AEC-VIZ and MI-VIZ successfully captured the surgical resection and may represent the wider extent of the EZ.

Patient 11

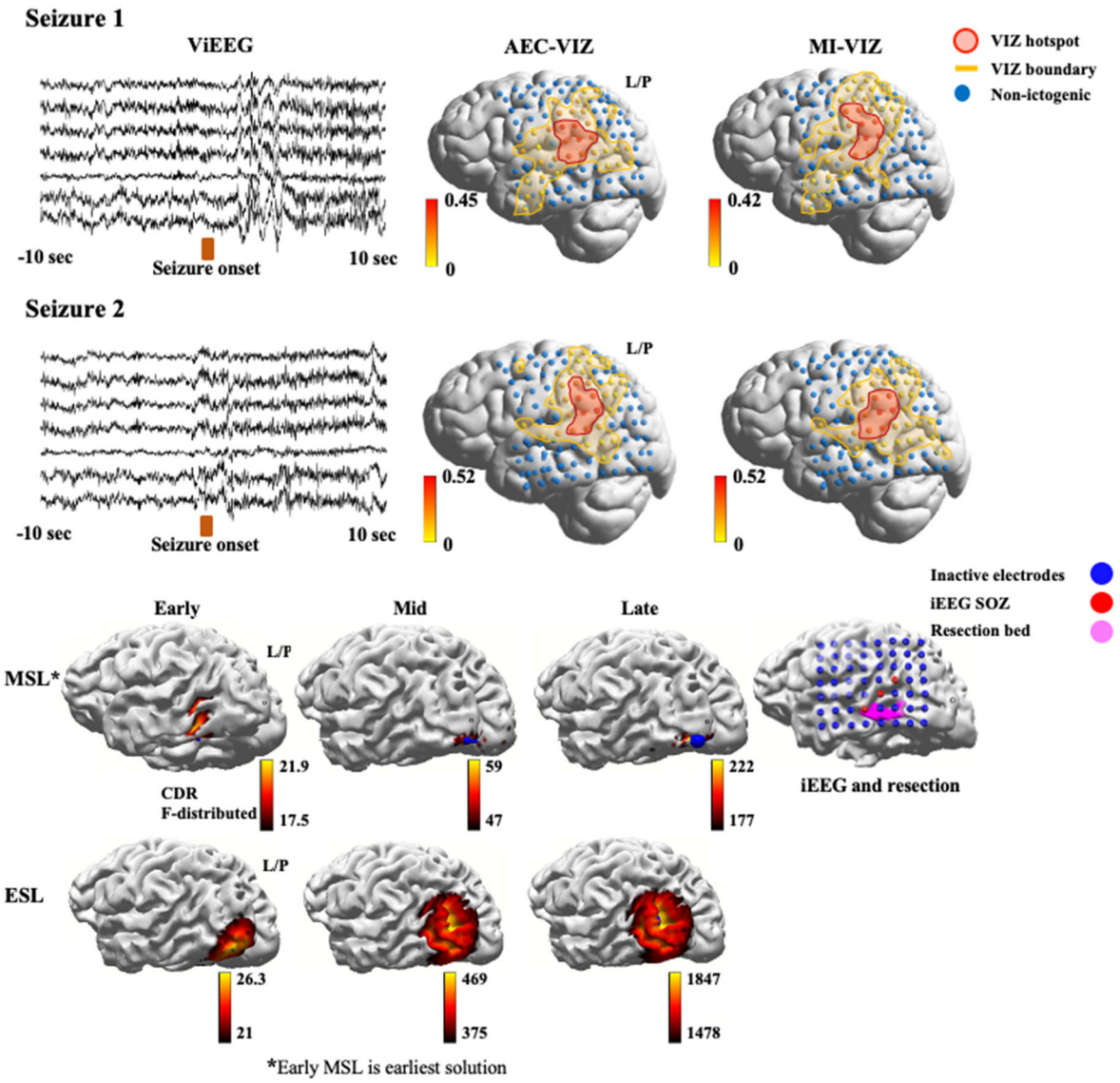

Supplementary Figure 14. Patient 11 had an extensive lesion at the left temporo-parieto-occipital (TPO) area on MRI with frequent disabling seizures (average 15 seizures per month) before surgery. Resection only gave an Engel III outcome. MEG sLORETA ictal early source localisation suggested a focus at the TPO junction. Guided by MSL solutions, ViEEGs were defined to extensively cover TPO junction and posterior frontal, superior parietal and lateral temporal areas. Source signals of two MEG captured seizure events are reconstructed. Ictal discharges can be seen in the representative ViEEG channels. Both AEC-VIZ and MI-VIZ identified hotspots (nodes in red line and shade) encompassing the left parieto-temporal convexity, with their boundaries including the TPO junction. AEC-VIZ and MI-VIZ from MEG data better concords with the earliest solution given by the MEG. This patient has achieved Engel III outcome with fewer disabling seizures. Based on surgical outcome, the MEG derived AEC-VIZ and MI-VIZ may represent the wider extent of the EZ. Indeed, the iEEG

SOZ was concordant with the VIZ solutions and extended beyond the limited resection zone. The resection area was limited by adjacent eloquent visual tracts.

Patient 12

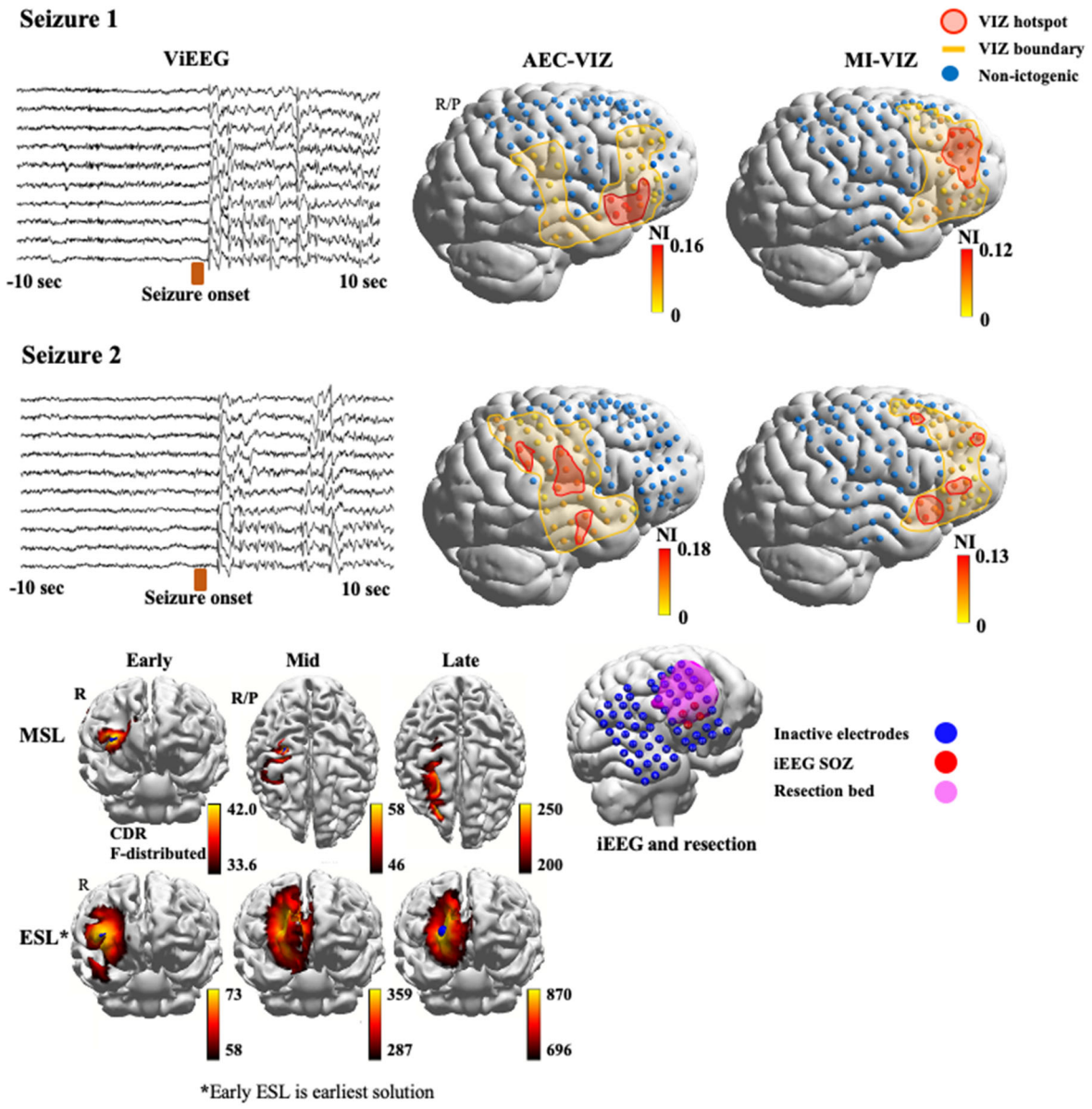

Supplementary Figure 15. Patient 12 had a large right frontal gliotic lesion with over 4 disabling seizures per month before resection which led to complete seizure freedom at 14 months. MEG sLORETA ictal early source localisation suggested a focus at right inferior frontal gyrus. Guided by MSL solutions, ViEEGs were defined to extensively cover right frontal, fronto-parietal and superior temporal areas. Source signals of two MEG captured seizure events are reconstructed. Ictal discharges can be seen in the representative ViEEG channels. Variability of hotspot and boundary results for AEC-VIZ and MI-VIZ is present across both seizures. MI-VIZ boundary from Seizure 1 and Seizure 2 fully contain the resection margin and the earliest solution given by the EEG rather than the MEG while MI-VIZ hotspot from Seizure 1 better predicts the EZ, iEEG SOZ and early-ESL (the earliest solution in this case). AEC-VIZ is discordant with the resection margin, iEEG SOZ and source

localisation solutions. This patient has achieved Engel I seizure-free outcome. Based on the seizure-free outcome, the MEG derived MI-VIZ successfully captured the EZ.

References

1. Goodfellow M, Rummel C, Abela E, Richardson MP, Schindler K, Terry JR. Estimation of brain network ictogenicity predicts outcome from epilepsy surgery. *Sci Rep* **6**, 29215 (2016).

2. Lopes MA*, et al.* An optimal strategy for epilepsy surgery: Disruption of the rich-club? *PLoS Comput Biol* **13**, e1005637 (2017).

3. Lopes MA*, et al.* Elevated Ictal Brain Network Ictogenicity Enables Prediction of Optimal Seizure Control. *Front Neurol* **9**, 98 (2018).

4. Palva JM*, et al.* Ghost interactions in MEG/EEG source space: A note of caution on inter-areal coupling measures. *Neuroimage* **173**, 632-643 (2018).

5. Schoffelen JM, Gross J. Source connectivity analysis with MEG and EEG. *Hum Brain Mapp* **30**, 1857-1865 (2009).

6. Kraskov A, Stogbauer H, Grassberger P. Estimating mutual information. *Phys Rev E Stat Nonlin Soft Matter Phys* **69**, 066138 (2004).

7. Rummel C*, et al.* Resected Brain Tissue, Seizure Onset Zone and Quantitative EEG Measures: Towards Prediction of Post-Surgical Seizure Control. *PLoS One* **10**, e0141023 (2015).

8. Enatsu R*, et al.* Usefulness of MEG magnetometer for spike detection in patients with mesial temporal epileptic focus. *Neuroimage* **41**, 1206-1219 (2008).

9. Oishi M*, et al.* Fusiform gyrus epilepsy: the use of ictal magnetoencephalography - Case report. *Journal of Neurosurgery* **97**, 200-204 (2002).

10. Plummer C, Vogrin SJ, Woods WP, Murphy MA, Cook MJ, Liley DTJ. Interictal and ictal source localization for epilepsy surgery using high-density EEG with MEG: a prospective long-term study. *Brain* **142**, 932-951 (2019).

11. Ruzich E, Crespo-Garcia M, Dalal SS, Schneiderman JF. Characterizing hippocampal dynamics with MEG: A systematic review and evidence-based guidelines. *Hum Brain Mapp* **40**, 1353-1375 (2019).

12. Brookes MJ*, et al.* A general linear model for MEG beamformer imaging. *Neuroimage* **23**, 936-946 (2004).

13. Handy TC. *Brain Signal Analysis: Advances in Neuroelectric and Neuromagnetic Methods*. The MIT Press (2009).

14. Van Veen BD, van Drongelen W, Yuchtman M, Suzuki A. Localization of brain electrical activity via linearly constrained minimum variance spatial filtering. *IEEE Trans Biomed Eng* **44**, 867-880 (1997).

15. Sekihara K, Hild KE, 2nd, Nagarajan SS. A novel adaptive beamformer for MEG source reconstruction effective when large background brain activities exist. *IEEE Trans Biomed Eng* **53**, 1755-1764 (2006).

16. Sekihara K, Nagarajan SS, Poeppel D, Marantz A. Asymptotic SNR of scalar and vector minimum-variance beamformers for neuromagnetic source reconstruction. *IEEE Trans Biomed Eng* **51**, 1726-1734 (2004).

17. Hillebrand A, Singh KD, Holliday IE, Furlong PL, Barnes GR. A new approach to neuroimaging with magnetoencephalography. *Hum Brain Mapp* **25**, 199-211 (2005).

18. Gramfort A*, et al.* MNE software for processing MEG and EEG data. *Neuroimage* **86**, 446-460 (2014).

19. Fischl B*, et al.* Whole brain segmentation: automated labeling of neuroanatomical structures in the human brain. *Neuron* **33**, 341-355 (2002).

20. Hincapie AS*, et al.* The impact of MEG source reconstruction method on source-space connectivity estimation: A comparison between minimum-norm solution and beamforming. *Neuroimage* **156**, 29-42 (2017).

21. Colclough GL, Woolrich MW, Tewarie PK, Brookes MJ, Quinn AJ, Smith SM. How reliable are MEG resting-state connectivity metrics? *Neuroimage* **138**, 284-293 (2016).

22. Akaike H. A new look at the statistical model identification. *IEEE Trans Automat Contr* **19**, 716-723 (1974).

23. Schwarz G. Estimating the Dimension of a Model. *Ann Stat* **6**, 461-464 (1978).